

## Permeability of polymeric scaffolds with defined pore micro-architecture and interconnectivity fabricated by solid freeform microprinting

<sup>1</sup>Kee-Won Lee, <sup>1\*</sup>Esmail Jabbari, <sup>1</sup>Lichun Lu, <sup>1</sup>Bradford L. Currier, <sup>2</sup>Joy Dunkers,  
<sup>2</sup>Martin Y. Chiang, <sup>2</sup>John A. Tesk, <sup>2</sup>Marcus Cicerone <sup>1</sup>Michael J. Yaszemski

<sup>1</sup>Department of Biomedical Engineering, Mayo Clinic College of Medicine,  
Rochester, MN, 55905

<sup>2</sup>Polymers Division, National Institute of Standards and Technology, Gaithersburg, MD 20899

\*Present address: Department of Chemical Engineering, University of South Carolina,  
Columbia, SC 29208

Three-dimensional (3D) microprinting is a computerized fabrication technique that can produce porous objects with highly complicated pore micro-architecture using data generated by computer aided design (CAD) or other imaging modalities [1]. This technique has been used for fabrication of porous biodegradable polymeric scaffolds that are intended, by design, to have reproducible and well-defined pores and connections for skeletal tissue engineering applications [2-4]. Scaffold porosity and interconnectivity are important design variables for tissue regeneration [5,6]. One measure related to pore interconnectivity is hydraulic permeability, the flow velocity through a porous material at a fixed pressure gradient [7]. The objective of this work was to study the effect of pore size and interconnectivity (defined as the fraction of cubic empty spaces connected to the outside air) on hydraulic permeability of polymeric scaffolds with well design-defined interconnectivity and pore micro-architecture.

Commercial CAD software was used to create the original scaffold models of the cubic orthogonal geometry with different pore sizes. Each pore with six faces was connected to the adjacent pores by 300  $\mu\text{m}$  diameter struts. These struts constituted the edges of the cubic lattice from which the pores were made. Opening-closing control of pores was implemented by closing a fraction of the pores of the original design randomly. All CAD data were converted to stereolithography (STL) files, imported to the 3D rapid prototyping machine, and printed by the PatternMaster's build-jet (polystyrene) and support-jet (wax) materials. The build-jet material was dissolved in acetone, which made a wax mold with pores in the space previously occupied by the polystyrene. Next, degradable poly(propylene fumarate) (PPF) polymerizing macromer was injected into the mold, and the polymerizing mixture was allowed to crosslink. Finally, a porous PPF scaffold was made by melting and removing the wax. Hydraulic conductivity was measured using the falling head conductivity test based on Darcy's law and hydraulic permeability was calculated by first multiplying the hydraulic conductivity by the viscosity of water, and then dividing the product by the specific weight of water.

As the pore size and the number of open pores were increased, porosity and hydraulic conductivity also increased. Porosities of PPF scaffolds with pore sizes of 600 and 900  $\mu\text{m}$  were very similar to the values predicted from the original CAD models. Micro Computerized Tomography ( $\mu\text{-CT}$ ) imaging of a 600  $\mu\text{m}$  pore scaffold (similar to the ones used in this permeability study) that was intended to have completely open connections between pores and with 600  $\mu\text{m}$  struts showed the structure to be open and with few defects (Fig. 1a). A pore size analysis of the reconstructed 3D scaffold resulted in a calculated porosity of  $(55 \pm 5) \%$  ( $\pm = u$ , the relative standard uncertainty of the mean of the porosity). The target porosity of the

CAD model was 50 %. A smoothed plot of one measure of the pore size distribution calculated from the  $\mu$ -CT images peaked near a pore with a radius of 650  $\mu\text{m}$ , which is quite close to the target of 600  $\mu\text{m}$  (Fig. 1b). The broad distribution of apparent pore sizes in Fig. 1b arises in part from the method of volume sampling in the image analysis method we used.

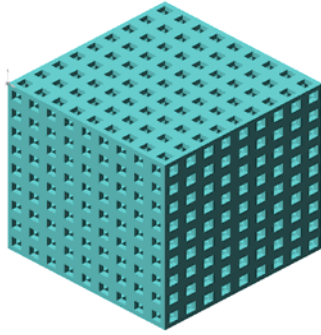


Fig.1a

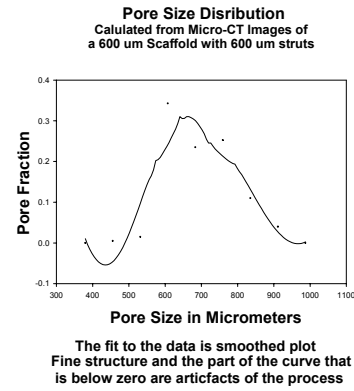


Fig.1b

Fig. 1a is a 3D view of a 600  $\mu\text{m}$  pore scaffold that is similar to the ones used, except that struts are 600  $\mu\text{m}$  thick. Micro-CT imaging analysis showed pores to be open and completely connected. The nominal distance from one edge of the scaffold to the opposite edge is 11 mm; distances between centers of the open, 600  $\mu\text{m}$ , connections are 1,200  $\mu\text{m}$ . Fig. 1b is a smoothed plot of pore fraction vs. pore size.

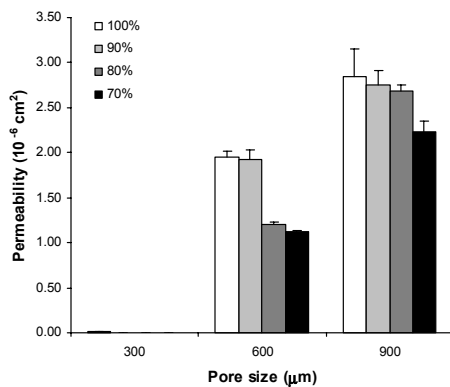


Fig. 2a

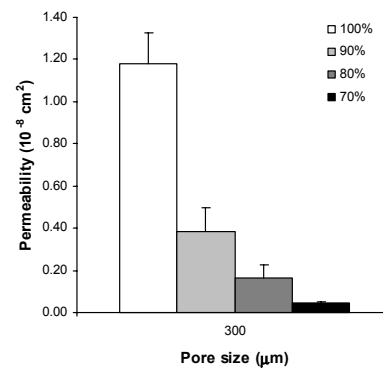


Fig. 2b

Fig. 2a is permeability data of PPF scaffolds with different pore interconnectivities 100 to 70 % and pore sizes of 300, 600, and 900  $\mu\text{m}$ . Fig.2b is permeability data of PPF scaffolds with a pore size of 300  $\mu\text{m}$  only.

As the degree of interconnectivity was decreased from 100 % to 70 %, hydraulic permeability decreased by a factor of  $10 \pm 0.5$ ,  $2 \pm 0.2$ , and  $1.3 \pm 0.1$  ( $\pm = u$ ) for nominal pore sizes of 300, 600, and 900  $\mu\text{m}$ , respectively (Fig. 2a). The permeability of scaffolds having a pore size of 300  $\mu\text{m}$  was particularly sensitive to changes in the interconnectivity. This may be

partly due to a small pore size that is close to the PatternMaster's minimum printable size of 250  $\mu\text{m}$ . In this case, the wax might not be completely removed and the remaining wax might be responsible for causing pore occlusion [8], especially as the number of closed pores increases and the ability to remove wax becomes increasingly difficult.

Our results reveal that hydraulic permeability depends on the micro-structure, such as pore size and pore interconnectivity, of polymeric scaffolds. Although fabrication of scaffolds with small pore sizes is still challenging, this new process can create shape specific biodegradable polymeric scaffolds with a design intended to produce well-defined reproducible micro-architectures for a variety of tissue engineering applications.

<sup>§</sup> Commercial products identified are neither endorsed nor recommended by NIST.

## References

1. Sachs, E., Cima, M., Williams, P., Brancazio, D., Cornie, J., Three dimensional printing: rapid tooling and prototypes directly from a CAD model, *J. Eng. Ind.* 114(4), 481-488, 1992.
2. Giordano, R. A., Wu, B. M., Borland, S. W., Cima, L. G., Sachs, E. M., Cima, M. J., Mechanical properties of dense polylactic acid structures fabricated by three dimensional printing, *J. Biomater. Sci. Polymer Edn.* 8(1), 63-75, 1996.
3. Lam, C. X. F., Mo, X. M., Teoh, S. H., Hutmacher, D. W., Scaffold development using 3D printing with a starch-based polymer, *Mater. Sci. Eng. C* 20(1-2), 49-56, 2002.
4. Park, A., Wu, B., Griffith, L. G., Integration of surface modification and 3D fabrication techniques to prepare patterned poly(L-lactide) substrates allowing regionally selective cell adhesion, *J. Biomater. Sci. Polymer Edn.* 9(2), 89-110, 1998.
5. Yang, S. F., Leong, K. F., Du, Z. H., Chua, C. K., The design of scaffolds for use in tissue engineering: part 1-traditional factors, *Tissue Eng.* 7(6), 679-689, 2001.
6. Leong, K. F., Cheah, C. M., Chua, C. K., Solid freeform fabrication of three-dimensional scaffolds for engineering replacement tissues and organs, *Biomaterials* 24, 2363-2378, 2003.
7. Agrawal, C. M., Ray, R. B., Biodegradable polymeric scaffolds for musculoskeletal tissue engineering, *J. Biomed. Mater. Res.* 55, 141-150, 2001.
8. Dunkers, J., Chiang, M.Y.M., Wang, X.F., Jabbari, E., Yaszemski, M., Dean, D., Wang, F., Tesk, J., Regnault, W., Kaplan, D., Reference scaffolds for characterization of porosity, *Proceedings of the Society for Biomaterials*, October 15-18, 2004, Philadelphia, abstr. 12.